



INSTITUT DE FRANCE  
Académie des sciences

# *Comptes Rendus*

---

## *Mécanique*

Kwassi Anani, Roger Prud'homme and Mahouton N. Hounkonnou

**An approximate analytical model for the frequency response of evaporating droplets under a mixed feeding regime**


Volume 351, Special Issue S2 (2023), p. 77-95

Published online: 20 February 2023

<https://doi.org/10.5802/crmeca.146>

**Part of Special Issue:** Physical Science in Microgravity within the Thematic Group  
Fundamental and Applied Microgravity

**Guest editors:** Olga Budenkova (CNRS, Université Grenoble Alpes, Grenoble INP, SIMaP, 38000 Grenoble, France), Catherine Colin (IMFT, Université de Toulouse, CNRS, INPT, UPS et GDR 2799 Micropesanteur Fondamentale et Appliquée) and Guillaume Legros (ICARE, CNRS UPR 3021, Univ. Orléans et GDR 2799 Micropesanteur Fondamentale et Appliquée)

 This article is licensed under the  
CREATIVE COMMONS ATTRIBUTION 4.0 INTERNATIONAL LICENSE.  
<http://creativecommons.org/licenses/by/4.0/>



*Les Comptes Rendus. Mécanique sont membres du  
Centre Mersenne pour l'édition scientifique ouverte*

[www.centre-mersenne.org](http://www.centre-mersenne.org)

e-ISSN : 1873-7234



---

Physical Science in Microgravity within the Thematic Group Fundamental and Applied Microgravity / *Sciences physiques en microgravité au sein du GDR Micropesanteur Fondamentale et Appliquée*

# An approximate analytical model for the frequency response of evaporating droplets under a mixed feeding regime

*Un modèle analytique approximatif pour la réponse en fréquence des gouttelettes d'évaporation sous un régime d'alimentation mixte*

Kwassi Anani<sup>a</sup>, Roger Prud'homme<sup>\*, b</sup> and Mahouton N. Hounkonnou<sup>c</sup>

<sup>a</sup> Laboratory of Mathematical Modelling and Applications, Department of Mathematics, University of Lomé, 02 BP 1515 Lomé, Togo

<sup>b</sup> Jean Le Rond d'Alembert Institute, UMR 7190 CNRS, Sorbonne University, 4 place Jussieu, 75252 Paris Cedex 05

<sup>c</sup> University of Abomey-Calavi, International Chair in Mathematical Physics and Applications (ICMPA-UNESCO Chair) 072 B.P. 050 Cotonou, Republic of Benin  
*E-mails:* [kanani@univ-lome.tg](mailto:kanani@univ-lome.tg) (K. Anani), [roger.prudhomme@sorbonne-universite.fr](mailto:roger.prudhomme@sorbonne-universite.fr) (R. Prud'homme), [norbert.hounkonnou@cipma.uac.bj](mailto:norbert.hounkonnou@cipma.uac.bj) (M. N. Hounkonnou)

**Abstract.** This work is one of the analytical approaches to evaluate the evaporation frequency response of injected droplets, using the Heidmann analogy of a single droplet that is continuously fed with the same liquid fuel. Based on a linear analysis using the Rayleigh criterion, a dimensionless response factor is determined. The effects due to the variation of the heat transfer coefficient of the feeding process, as well as those due to the characteristic evaporation times and phase delay are analyzed. An abrupt increase of the response factor occurs, when a thermodynamic coefficient of the injected fuel takes certain specific values.

**Résumé.** Ce travail est l'une des approches analytiques pour évaluer la réponse en fréquence d'évaporation des gouttelettes injectées, en utilisant l'analogie de Heidmann i.e. d'une seule gouttelette alimentée en continu avec le même carburant liquide. Sur la base d'une analyse linéaire utilisant le critère de Rayleigh, un facteur de réponse sans dimension est déterminé. Les effets dus à la variation du coefficient de transfert de chaleur du processus d'alimentation, ainsi que ceux dus aux temps caractéristiques d'évaporation et au retard de phase sont analysés. Une augmentation brutale du facteur de réponse se produit, lorsqu'un coefficient thermodynamique du carburant injecté prend certaines valeurs spécifiques.

---

\* Corresponding author.

**Keywords.** Combustion instability, Injection regime, Evaporation, Double confluent Heun equation, Transfer function.

**Mots-clés.** instabilité de combustion, régime d'injection, évaporation, équation de Heun à double confluence, fonction de transfert.

*Published online: 20 February 2023*

## 1. Introduction

Combustion instabilities are still nowadays a challenging area in combustion research, though their modeling and control have been investigated in many published works by various research teams during the past decades. These instabilities result from the coupling between acoustic waves and combustion. In confined devices, the coupling between acoustic field and heat or mass release at certain frequency levels may lead to engine failure or other catastrophic consequences [1, 2]. On the contrary, new blends of fuels can be engineered to undergo preferential instabilities leading to homogeneous combustion with higher efficiency [3]. Combustion instabilities can occur in both premixed and diffusion flames. The present study is concerned with subcritical diffusion flame models. In these latter, many causes were identified as being responsible for exciting or damping the mass release frequency response [4, 5]: period of ambient pressure oscillations that is closely related to the combustion chamber geometry, liquid fuel injection and atomization mechanisms with diverse boundary conditions, vaporization characteristic times that are obviously dependent on thermal convection and conduction processes, etc.

In comparison with other processes that take place inside the combustion chamber, the vaporization process has been pointed as the slowest [6], and hence may be the rate-controlling process. The evaporating mass frequency response of droplets to ambient pressure oscillations are generally computed by using classical droplet evaporation theories [3], on the basis of the Rayleigh criterion [7], by assuming simplifying assumptions. Many of the theoretical studies in the area are based on a single vaporizing droplet model as in [6, 8, 9]. Then, by means of numerical simulations, it is observed that the frequency response of spray droplets to ambient pressure oscillations can be considered as a statistical consequence of the vaporization characteristics of each individual droplet in the array. Among previous numerical works on vaporization frequency response of sprays, Tong and Sirignano [10] examined the effects of oscillating gas pressure and velocity on vaporization rates of continuously injected droplets during combustion instability. They concluded that self-sustained acoustical oscillations can occur in the combustor when vaporization is a controlling phenomenon. More recently, de la Cruz Garc'ia et al. [11] investigated on the self-excited oscillations in a kerosene spray flame and concluded that the combustor stability strongly depends on the fuel distribution, degree of evaporation, and mixing before the main reaction zone. A progress has also been made in analytical modeling of vaporization frequency response of spray droplets. Haddad and Majdalani [12] provided a closed-form analytical solution for the transverse vorticoacoustic wave in a circular cylinder with headwall injection. Likewise, researchers have recently reported improved analytical models for spray combustion instability in diverse configurations as for example Greenberg and Katoshevski (see [13] and references therein).

One of the theoretical approaches for analyzing the evaporating mass frequency response to pressure oscillations of a spray of repetitively injected drops into a combustion chamber, can be considered from the Heidmann analogy of a spherical vaporizing droplet [14]. According to the Heidmann analogy, a single stationary spherical droplet represents this vaporizing spray of droplets. This mean droplet is a vaporizing droplet, continuously fed with the same liquid fuel, so that its volume is assumed to remain almost constant during the vaporization process. This

configuration consists of representing the spray of repetitively injected drops in the combustion chamber by a motionless mean droplet. The influence of spatial gas pressure and velocity variations, which are inherent to acoustic modes, are not taken into account with this approach, e.g. in the case of transverse acoustic modes to which the spray can be submitted, because this approach is focused on the behavior of droplets located at pressure anti-nodes. The single vaporizing droplet is continuously supplied at a stationary flow rate with the same liquid fuel. This classical model can permit to include most of the above-mentioned mechanisms that intervene in combustion instability phenomena, in a single theoretical analysis. Heidmann and Wieber first based their model on the hypothesis that, the mean spherical droplet summarizes the oscillatory rate of vaporization of an array of repetitively injected droplets in the combustion chamber [14]. However, they assumed an infinite thermal diffusivity of the liquid phase, therefore the mean droplet has a uniform temperature whatever the feeding process adopted.

This classical model was refined by Prud'homme et al. [15], especially at ONERA (the French Aerospace Laboratory) and within the framework of the research group GDR-MFA (Micropesanteur Fondamentale et Appliquée). This group leads a program on micro gravity in the field of engineering sciences with the assistance of the main research structures of the French State, namely the CNRS and the CNES. The present study is part of the celebration of the 30 years since the creation of this research group. During their first work, Prud'homme et al. [15] took into account a finite thermal diffusivity of the liquid, but the feeding process at the mean droplet center was assumed adiabatic, and the radial thermal convection term that appears in the energy equation of the liquid phase was neglected (pure conduction model). In [16], Anani and Prud'homme extended the study of this pure conduction model by taking into account the isothermal feeding process at the mean droplet center. More recently, an approximate analytical model has been realized by Anani et al. [17], where has been abandoned the simplifying assumption of negligible radial thermal convection effect inside the liquid phase. Nevertheless, only the two extreme cases of center injection that are the adiabatic and the isothermal feeding regimes were considered. Apart from this latter work, no analytical solution has been found nor any asymptotic study has been performed for intermediate injection cases, where the feeding regime at the mean droplet center is an intermediate case between the two extreme thermal forcing types.

Taking into account the mixed or generalized injection regime at the center of the mean droplet, this paper aims to contribute to the linear analysis of subcritical combustion instabilities by analytical approaches based on the mean spherical droplet configuration as in [17]. In Section 2, a brief description is given of the unperturbed state corresponding to the vaporization of the continuously fed spherical droplet in a stable environment. In Section 3, the linear analysis for harmonic perturbations in pressure is performed and a double confluent Heun equation (see [18]) is derived from the energy equation of the liquid phase. Then, an approximate analytical expression of the temperature field inside the mean droplet is obtained for the generalized or mixed injection regime and the mass response factor is defined. Results are discussed in Section 4. Throughout the discussion, comparisons are made with the results of other combustion instability models found in the literature that account for the vaporization of individual droplets injected into the spray. Finally, key results are recalled in the conclusions.

## 2. Description of the stabilized state

### 2.1. Model assumptions

Individual fuel droplets are repetitively injected into a subcritical combustion chamber such that the interaction between the droplets or between the droplets and the wall are negligible. Velocity-stabilized hypotheses are assumed as in [14], and an idealized physical configuration of a mean

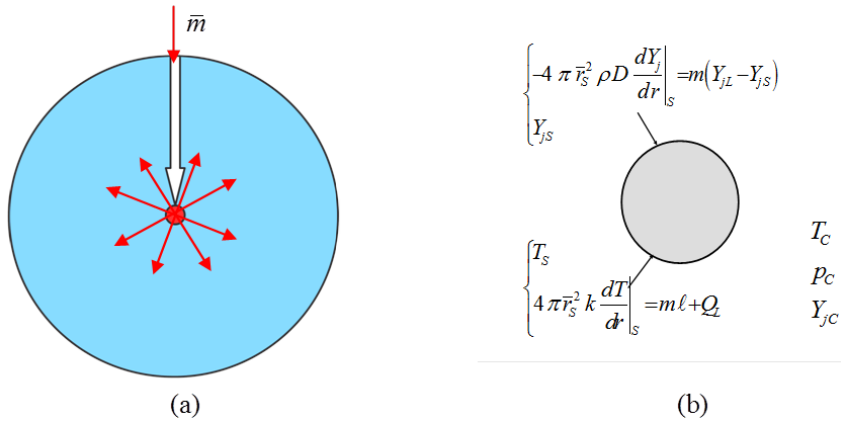


**Figure 1.** (a) The mean vaporizing droplet, continuously fed by a point source placed at its center. (b) Boundary conditions for the supplied droplet.

spherical droplet at rest in the combustion chamber, here represents the vaporizing spray of droplets. In the present model, the feeding is realized at some liquid-liquid heat transfer coefficient by using a source point placed at the spherical droplet center, in such a way that only radial thermal convection and conduction effects are taken into account inside the mean droplet during the process. This feeding process is now considered as a proper boundary condition, that is a mixed or a generalized feeding regime controlling the actual process of liquid fuel injection into the combustion chamber. Thus, the frequency response of individual drops in the spray is supposed to be summarized by the mean droplet, which is placed at a specific location in the combustion chamber (pressure anti-node and velocity node). As the instantaneous evaporating mass  $m$  of the mean droplet is continuously restored with the average mass flow rate  $\bar{m}$  of the same fluid, an almost constant radius  $\bar{r}_S$  is assumed for the vaporizing mean droplet during the process time. The choice of the Arithmetic Mean Diameter configuration for the mean droplet leads to conservation equations with fixed boundary conditions and is motivated by the analytical approach of the problem. From now on, all barred quantities denote mean values corresponding to the stabilized state, whereas all primed quantities will indicate relative perturbation quantities, i.e.  $x' = (x - \bar{x})/\bar{x}$ .

The feeding process is realized by using a point source placed at the droplet center in such a way that the local feeding rate is distributed throughout the droplet (see Figure 1(a)). Except for the radial thermal convection effect from the droplet center to its evaporation surface, any other convective transport or liquid recirculation phenomenon within the droplet will be assumed negligible. The thermal conductivity  $k_L$ , the density  $\rho_L$  and the specific heat  $c_L$  of the droplet will be treated as constant. The spherical shape of the mean droplet is maintained at every moment during the process, and the thermal dilatation of the liquid is negligible. At the mean droplet center, a mixed injection regime is considered, that is, the liquid fuel is injected into the droplet with a positive heat transfer coefficient  $h$ . The two extreme cases of this generalized boundary condition are the adiabatic feeding regime ( $h = 0$ ), where a zero temperature gradient is assumed at the droplet center, and the isothermal feeding regime ( $h = +\infty$ ), where the droplet center is kept at the constant temperature  $\bar{T}_S$ . This latter represents the mean value of  $T_S$ , the spatially uniform but time-varying temperature of the saturated vapor at the surface of the stabilized droplet.

Around the droplet surface, the gas phase evolves in a quasi-steady state. There is no gas diffusion into the droplet and equilibrium conditions are assumed at the droplet/gas interface for the stabilized state. Far from the mean droplet, the ambient environment of the chamber is at a constant subcritical temperature  $T_C$  and pressure  $p_C$ . These boundary conditions are shown on Figure 1(b), where subscripts  $L$  and  $l$  indicate the liquid phase while the round letter  $\ell$  will be used throughout the document to denote the latent heat of vaporization per unit mass of liquid. The subscripts  $S$  and  $C$  refer respectively to the droplet surface and to the ambient conditions in the combustion chamber far from the droplet. The quantity  $Q_L$  designates the heat flux transferred to the liquid and  $D$  denotes the binary diffusion coefficient of the fuel vapor in air. The thermal conductivity and the density of the gas mixture around the droplet surface are respectively denoted by  $k$  and  $\rho$ . The gaseous mixture at the immediate vicinity of the droplet is made up of fuel species  $j = F$  and of combustion products diluted species  $j = A$  proceeding from the flame front at infinity. The mass fraction of species  $j$  is denoted by  $Y_j$ . For reason of simplicity, a mono-component droplet with only fuel species will be considered, that is  $Y_{FL} = 1$  and  $Y_{AL} = 0$ .

Theoretical studies of the evaporating mass response of spray droplets to acoustic and/or velocity perturbations in combustors are mostly based on numerical simulations. But, even when assuming certain simplifying assumptions, analytical models that include more complex aspects of the problem are needed for providing deep insights in the vaporization frequency response. Nevertheless, both numerical and analytical models need to be confronted with appropriate experimental measurements and more detailed databases for validating the predictions. As stated in [19], specifications of an experimental design may include several regulations and measurement devices. Since the present theoretical study is based on the mean droplet configuration, experimental facility and methods similar to those described in [20] can provide tracks for some experiments. However, the problem is here considered only under its analytical aspect. As mentioned in the introduction, the mean droplet model can permit to include in a single theoretical analysis most of the mechanisms that intervene in spray combustion instability. The results obtained may then serve as references for full experimental and numerical simulations of sprays combustion instabilities, which will not necessarily need to rely on the simplifying assumptions adopted here.

The present model of a representative drop, continuously fed by a mass and thermal point source placed in its center, allows to include among other advantages, the possibility to formulate the boundary conditions with a heat transfer coefficient. But, unlike the classical adiabatic condition, the generalized boundary conditions do not ensure the regularity of the heat fluxes at the center. Even in the adiabatic feeding regime, the radial velocity of the liquid diverges at the center of the mean droplet, where its infinite value is counterbalanced by zero heat flux at the center. In all cases, in the adiabatic or mixed feeding regimes, the evaluation of the mass response factor depends only on the regularity of the temperature flux at the surface of the mean droplet, and this condition will be well verified here in all the different feeding regimes. Thus, using simplifying assumptions, the present study aims to provide regular approximate solutions, in order to investigate the effects of the heat transfer coefficient of the fuel injection process, on the frequency response of the vaporization.

## 2.2. Evaporation characteristic times

The residence time and the transfer time by thermal diffusion are the two characteristic times controlling heat transfer processes inside the stabilized mean droplet. The residence time of the continuously fed droplet replaces the notion of a free droplet lifetime in the present situation of almost constant volume and can be identified to the ratio  $\bar{\tau}_v = \bar{M}/\bar{m}$ . Here,  $\bar{m}$  is the stationary feeding rate, while  $\bar{M}$  represents the mean value of the actual mass  $M$  of the supplied droplet.

The transfer time by thermal diffusion process is identified to  $\bar{\tau}_T = \bar{r}_S^2 / \kappa_L$ , where  $\bar{r}_S$  is the average radius of the mean droplet and  $\kappa_L = k_L / (\rho_L c_L)$  is the thermal diffusivity of the liquid. The timescale ratio  $\theta = 9\bar{\tau}_v / \bar{\tau}_T = \bar{\tau}_v / \tilde{\tau}_T$ , where  $\tilde{\tau}_T = \bar{\tau}_T / 9$ , will be called the thermal exchange ratio or more briefly the exchange ratio from now on. It is of the same order of magnitude as  $1/P_L$ , where  $P_L$  is the Péclet number of the liquid phase. The coefficient 9, which appears in this ratio will lead hereafter to a more simple expression of the transfer function. It will be also kept for results comparison purposes with previous mean droplet models as in [16, 17]. During the vaporization process, instabilities related to intrinsic or external pressure oscillations can cause departure from the stabilized-state conditions and a linear analysis can be performed in the case of harmonic perturbations in pressure. A major characteristic time of the perturbed state of the mean droplet is the oscillation or wave period of the ambient pressure. The angular frequency of the harmonic oscillations in pressure will be denoted by  $\omega$ . In [14], the mass response factor was studied over a wide range of flow conditions and the data was found to be correlated with some dimensionless parameter, that is the droplet lifetime or half lifetime normalized by the wave period. Likewise, in the present study, a reduced frequency  $u$  depending on the residence time  $\bar{\tau}_v$  is defined as  $u = 3\omega\bar{\tau}_v$ .

### 2.3. Equations for the stabilized state

The mass balance of the mean evaporating droplet is written:

$$\frac{dM}{dt} = \bar{m} - m, \quad (1)$$

where  $\bar{m}$  and  $m$  denote respectively the stationary flow of injection and the instantaneous flow of evaporation. In the unperturbed or stabilized state, equation (1) becomes:  $dM/dt = 0$ , implying  $\bar{m} = m$  and  $M = \bar{M}$ . The instantaneous amount of heat  $Q_L$  penetrating into the droplet can be evaluated as:

$$Q_L = Q - m\ell = 4\pi\bar{r}_S^2 k_L \frac{\partial T_l}{\partial r} (r = \bar{r}_S, t), \quad (2)$$

where  $T_l(r, t)$  is the droplet temperature at radial coordinate  $r$  and at time  $t$ ,  $Q$  is the external gas heat flow and  $\ell$  is the latent heat of vaporization per unit mass of the liquid. Equation (2) couples the gas and the liquid phase solutions at the droplet surface. Since both radial thermal convection and conduction data need to be appropriately included in the formulation of the energy conservation equation, the internal temperature  $T_l \equiv T_l(r, t)$  verifies the following equation:

$$\rho_L c_L \frac{\partial T_l}{\partial t} + \rho_L c_L v_r \frac{\partial T_l}{\partial r} - \frac{k_L}{r} \frac{\partial^2 (r T_l)}{\partial r^2} = 0, \quad (3)$$

where  $v_r$  is the central injection velocity expressed as  $v_r = \bar{m} / 4\pi\rho_L r^2$  for  $0 < r < \bar{r}_S$ . Equation (3) is subject to a mixed boundary condition at the droplet center and to the Dirichlet boundary condition at the surface:

$$\begin{cases} \frac{\partial T_l}{\partial r}(r=0, t) = \frac{h}{\bar{r}_S} (T_l(0, t) - \bar{T}_S), \\ T_l(\bar{r}_S, t) = T_S(t). \end{cases} \quad (4)$$

The parameter  $h > 0$  in conditions (4) indicates the heat transfer coefficient. We recall that,  $h = 0$  for the adiabatic injection regime and the boundary condition at the droplet center is reduced to  $\partial T_l / \partial r = 0$  on  $r = 0$ , whereas  $h = +\infty$  for the isothermal injection regime and the related condition at the droplet center becomes  $T_l(0, t) = \bar{T}_S$ . The mixed boundary condition at the droplet center can then be viewed as an idealized modeling of a preheated spray injection process. In liquid fuel injection processes, internal flow evaluations depend on inlet boundary conditions (see [21] and references therein). Some studies have shown that the reduction in kinematic viscosity resulting from fuel preheating improves the combustion and emissions performance of the

engine [22,23]. Now, in subcritical combustion systems, the two extreme cases bounding the possible range of real inlet liquid temperature fluxes are precisely the adiabatic and the isothermal feeding regimes. The adiabatic feeding regime at the mean droplet center can be related to an unheated spray feeding process, where the mean temperature  $\bar{T}_A$  of the injected fuel is connected to standard conditions for temperature and pressure. On the contrary, the isothermal feeding regime can be brought closer to the process of injection of fuel at temperature  $\bar{T}_S$ . The latter is related to the liquid wet bulb temperature  $\bar{T}_{WB}$  or to its boiling temperature  $\bar{T}_B$ , when  $\bar{T}_{WB}$  estimate is unavailable (see [24]). Therefore, in an actual mixed injection process, the inlet fuel temperature may be stated between the extreme values that are  $\bar{T}_A$  and  $\bar{T}_S$ . In brief, during the spray vaporization process, the corresponding rate of heat brought by the injected fuel to the array of droplets is here investigated by means of the heat transfer coefficient  $h$ .

Assuming the classical quasi-steady hypothesis of a local evaporation equilibrium at the surface of the mean droplet, the instantaneous mass vaporization rate can be evaluated as:

$$m = 2\pi\rho D r_S Sh^* \ln(1 + B_M) = 4\pi \frac{k}{c_p} r_S Nu^* \ln(1 + B_T), \quad (5)$$

where  $B_M = (Y_{FS} - Y_{FC})/(1 - Y_{FS})$  and  $B_T = c_p(T_C - T_S)/(\ell + Q_L/m)$  represent respectively the mass and heat transfer numbers of Spalding, and  $c_p$  denotes the specific heat capacity of fuel vapor at constant pressure. The parameters  $\rho$ ,  $k$  and  $D$  are here recalled as the density, the thermal conductivity and the binary diffusion coefficient of the mixture of vapor and ambient gas. The Nusselt and Sherwood numbers  $Nu^*$  and  $Sh^*$  were provided in the extended film model by Abramzon and Sirignano [25]. The saturated vapor pressure at the droplet surface is expressed as  $p_{sat}(T_S) = \exp(a - b/(T_S - c))$ , where  $a$ ,  $b$  and  $c$  are coefficients related to the fuel thermophysical properties. The mole fraction  $X_{FS}$  of fuel species is connected to the saturated vapor pressure  $p_{sat}$  by the relation  $p X_{FS} = p_{sat}(T_S)$ , where  $p = p_C$  is the ambient pressure. The mass fraction  $Y_{FS}$  of the vapor at the droplet surface can be expressed as a function of the mole fraction  $X_{FS}$  by:

$$Y_{FS} = \frac{\mathcal{M}_F}{\mathcal{M}_F X_{FS} + \mathcal{M}_A X_{AS}} X_{FS}, \quad (6)$$

with  $\mathcal{M}_j$  denoting the molecular weight of species  $j = A$  for combustion products diluted species, or  $j = F$  for fuel species. Temperature and concentration values continually evolve in the gas phase and their averaged values can be respectively taken at some reference temperature  $\bar{T} = T_S + A_r(T_C - T_S)$  and concentration  $\bar{Y}_j = Y_{jS} + A_r(Y_{jC} - Y_{jS})$  with  $A_r = 1/3$ . Here, the Lewis number  $Le = k/\rho D c_p$  is assumed equal to 1 and both  $Sh^*$  and  $Nu^*$  are equal to 2.

### 3. Linear analysis for harmonic perturbations

#### 3.1. Linear analysis of the liquid-phase

In order to perform a linear analysis, each flow variable  $f$  is divided into steady and unsteady parts by writing  $\Delta f = f - \bar{f}$ , where  $\bar{f}$  is the mean value,  $\Delta f$  is the absolute perturbation of the flow, and  $f' = \Delta f / \bar{f}$  is the corresponding relative perturbation. Thus, the relative perturbation of the droplet temperature field is  $T'_l(r, t) = [T_l(r, t) - \bar{T}_l(r, t)] / \bar{T}_l(r, t)$ , and the linearized form of the heat flow penetrating into the droplet (see equation (2)) will read:

$$4\pi \bar{r}_S^2 k_L \bar{T}_S \frac{\partial T'_l}{\partial r}(r = \bar{r}_S, t) = Q_L - \bar{Q}_L = Q_L = \Delta Q_L \quad (7)$$

since  $\bar{Q}_L = 0$ . The energy conservation equation (equation (3)) becomes in its perturbed form:

$$\frac{\partial(r T'_l)}{\partial t} + \kappa_L \left( \frac{3\bar{r}_S}{\theta r} \frac{\partial T'_l}{\partial r} - \frac{\partial^2(r T'_l)}{\partial r^2} \right) = 0, \quad (8)$$



where  $\theta = \bar{\tau}_v / \bar{\tau}_T$  is the thermal exchange ratio as defined in Subsection 2.2. From equations (4), the boundary conditions at the perturbed state are deduced as:

$$\begin{cases} \frac{\partial T'_l}{\partial r}(r=0, t) = \frac{h}{\bar{r}_S} T'_l(0, t), \\ T'_l(\bar{r}_S, t) = T'_S. \end{cases} \quad (9)$$

In the case of harmonic perturbations in pressure of frequency  $\omega$ , the relative perturbation of the flow variable  $f$  takes the form of  $f' = \Delta f / \bar{f} = \hat{f}(r) e^{i\omega t}$ . The parameters as ambient pressure, temperature and heat transferred into the droplet are respectively perturbed as  $p'_C = \hat{p}_C e^{i\omega t}$ ,  $T'_l = \hat{T}_l(r) e^{i\omega t}$  and  $\Delta Q_L = \Delta \hat{Q}_L(r) e^{i\omega t}$ . The perturbed form of the energy conservation equation (equation (8)) can now be written as follows:

$$i r^2 \omega \hat{T}_l + \frac{3\kappa_L \bar{r}_S}{\theta} \frac{d\hat{T}_l}{dr} - \kappa_L r \frac{d^2(r\hat{T}_l)}{dr^2} = 0. \quad (10)$$

Or by equivalence as:

$$i\omega \bar{\tau}_T \xi \hat{T}_l + \frac{1}{3\theta \xi} \frac{d\hat{T}_l}{d\xi} - \frac{d^2(\xi \hat{T}_l)}{d\xi^2} = 0, \quad (11)$$

where  $\hat{T}_l$  is rather written as a function of the reduced radius variable  $\xi = r / \bar{r}_S$ , with  $0 < \xi < 1$ . In connection with  $\xi$ , equations (9) expressing the boundary conditions in the mixed or generalized feeding regime will read:

$$\begin{cases} \frac{d\hat{T}_l}{d\xi}(\xi=0) = \frac{h}{\bar{r}_S} \hat{T}_0 \\ \hat{T}_l(1) = \hat{T}_S, \end{cases} \quad (12)$$

where  $\hat{T}_0$  is the temperature of the preheated liquid fuel injected at the droplet center.

We now consider the conjugate complex numbers

$$s_0 = (1+i)(\omega/2\kappa_L)^{1/2} \quad \text{and} \quad \bar{s}_0 = (1-i)(\omega/2\kappa_L)^{1/2},$$

obtained from equation (11) by using the two roots  $s_0$  and  $-s_0$  of the characteristic equation  $i\omega - \kappa_L s^2 = 0$ , when neglecting the convective term  $(3\kappa_L \bar{r}_S / \theta) d\hat{T}_l / dr$ . A solution of equation (11) subject to equations (12), can be sought in the form of  $\xi \hat{T}_l(\xi) = J(\xi) \{1 - \cos[\bar{s}_0 \bar{r}_S \xi \exp(i \arctan h)]\}$ , with  $\exp(i \arctan h) = (ih+1)/(h^2+1)^{1/2}$ , where  $h$  is the heat transfer coefficient,  $J$  refers to a function to be determined and  $\exp(i \arctan h) = (ih+1)/(h^2+1)^{1/2}$ . Writing  $S_0 = \bar{s}_0 \bar{r}_S \exp(i \arctan h)$  and substituting the functions  $\sin(S_0 \xi)$  and  $\cos(S_0 \xi)$  in equation (11) by their truncated expansions of second order, that are  $\sin(S_0 \xi) \approx S_0 \xi$  and  $\cos(S_0 \xi) \approx 1 - (S_0 \xi)^2 / 2$ , the expression  $\xi J$  should approximately verify the following double confluent Heun equation:

$$\frac{\xi^2 d^2(\xi J)}{d\xi^2} + \left(2\xi - \frac{3}{\theta}\right) \frac{d(\xi J)}{d\xi} - 2\bar{s}_0^2 \bar{r}_S^2 \frac{h(i-h)}{h^2+1} \xi^2(\xi J) = 0. \quad (13)$$

Now, using the notations of the Maple software, the solution of equation (13) can be expressed as  $J(\xi) = C_0 \exp[-3(\theta \xi)^{-1}] \text{HeunD}(x_1, x_2, x_3, x_4, x) / \xi^{5/2}$ , where  $C_0$  is a constant to be determined and  $\text{HeunD}(x_1, x_2, x_3, x_4, x)$  is the double confluent Heun function. In this latter function, the variable  $x$  is expressed as function of  $\xi$  by  $x = (\xi^2 - 1) / (\xi^2 + 1)$  and the four related parameters  $x_1, x_2, x_3$  and  $x_4$  are respectively given as:

$$\begin{aligned} x_1 &= 0, \\ x_2 &= -[\theta^2(h^2+1) - 9 - 9h^2 - 24uh(ih+1)\theta] / 4\theta^2(h^2+1), \\ x_3 &= -[9 + (9 - 24iu\theta)h^2 - 24hu\theta] / 2\theta^2(h^2+1) \\ \text{and } x_4 &= -[-\theta^2(h^2+1) - 9 - 9h^2 - 24uh(ih+1)\theta] / 4\theta^2(h^2+1). \end{aligned}$$

Here, the parameter  $u = 3\omega\bar{\tau}_v$  is the reduced frequency of the ambient pressure as defined in the Subsection 2.2. The constant  $C_0$  is determined by using the boundary condition at the mean droplet surface,  $\hat{T}_l(1) = \hat{T}_S$ . This leads to the expression of an approximate analytical solution of equation (11) as:

$$\hat{T}_l(\xi) = \frac{\hat{T}_S \{1 - \cos[\bar{s}_0 \bar{r}_S \xi \exp(i \arctan h)]\}}{\{1 - \cos[\bar{s}_0 \bar{r}_S \exp(i \arctan h)]\} \xi^{5/2}} \exp\left[\frac{3}{2\theta} \left(1 - \frac{1}{\xi}\right)\right] \times \text{HeunD}\left(x_1, x_2, x_3, x_4, \frac{\xi^2 - 1}{\xi^2 + 1}\right). \quad (14)$$

Except for the case where the temperature gradient is null at the droplet center ( $h = 0$ ), the solution (14) presents an essential discontinuity at  $\xi = 0$  once  $h > 0$ . Nevertheless, only the regularity condition at the droplet surface ( $\xi = 1$ ) is needed for the calculation of the mass response factor and this condition is well verified by the equation (14).

The flow condition at the droplet surface (equation (7)) can be expressed as function of the reduced radius  $\xi = r/\bar{r}_S$ , and then be applied to the solution (14). This will lead to:

$$\Delta \hat{Q}_L = -4\pi \bar{r}_S k_L \bar{T}_S \hat{T}_S E(u, \theta, h), \quad (15)$$

where the function  $E$  is expressed with the parameters  $u$ ,  $\theta$  and  $h$  as:

$$E(u, \theta, h) = \frac{\bar{s}_0 \bar{r}_S \exp(i \arctan h) \sin[\bar{s}_0 \bar{r}_S \exp(i \arctan h)]}{\cos[\bar{s}_0 \bar{r}_S \exp(i \arctan h)] - 1} - \frac{3}{2\theta} + \frac{5}{2}. \quad (16)$$

With  $u = 3\omega\bar{\tau}_v$  and  $\theta = \bar{\tau}_v/\bar{\tau}_T$ , the calculations give  $\bar{s}_0 \bar{r}_S = (1 - i)(3u/2\theta)^{1/2}$ .

### 3.2. The linearized equations of the gas phase

The linearized equations for the liquid/gas interface were first presented in [15] and were used in [16, 17]. Introducing the harmonic perturbations in the flow variables, the perturbed mass flow rate and ambient pressure respectively become  $m' = \hat{m}e^{i\omega t}$  and  $p'_C = \hat{p}_C e^{i\omega t}$ . In consequence, the linearized equations were obtained from the stabilized state equations of the gas phase (see Subsection 2.3) as follow:

$$\hat{m} = \alpha \frac{i u}{1 + i u} (\bar{b} \hat{T}_S - \hat{p}_C), \quad (17)$$

and

$$\Delta \hat{Q}_L = \bar{m} \bar{\ell} (\bar{a} \hat{p}_C - \mu \hat{T}_S). \quad (18)$$

The different coefficients involved in these equations were expressed as:

$$\bar{a} = \frac{\bar{T}_C}{\bar{T}_C - \bar{T}_S} \frac{\gamma - 1}{\gamma} + \varphi, \quad \bar{b} = \frac{\bar{T}_S}{(\bar{T}_S - c)^2} b, \quad \mu = \frac{\bar{T}_S}{\bar{T}_C - \bar{T}_S} - \frac{2c}{\bar{T}_S - c} + \bar{b}\varphi$$

and

$$\alpha = \frac{\bar{B}_M}{(1 + \bar{B}_M) \ln(1 + \bar{B}_M)} \varphi, \quad \text{where} \quad \varphi = \frac{\bar{Y}_{AC} \bar{Y}_{FS}}{\bar{Y}_{AS} (\bar{Y}_{FS} - \bar{Y}_{FC})} \frac{\mathcal{M}_F}{\mathcal{M}_F \bar{X}_{FS} + \mathcal{M}_A \bar{X}_{AS}}.$$

The parameter  $\gamma$  denotes the constant isentropic coefficient, while the latent heat of vaporization per unit mass of the liquid is given by  $\ell = bRT_S^2/\mathcal{M}_F(T_S - c)^2$ , with  $R$  standing for the universal gas constant.

### 3.3. Mass response factor

The mean spherical droplet is assumed to be at rest in the combustion chamber and its velocity response can be neglected. Only the evaporating mass response due to the ambient acoustic forcing will here be considered. According to the Rayleigh criterion, the oscillations in pressure  $p' = (p - \bar{p})/\bar{p}$  induces a perturbation in the evaporating mass flow rate  $q' = (q - \bar{q})/\bar{q}$ . The resulting mass response factor  $N$  can then be expressed as the ratio of the magnitude of the mass perturbation to that of the pressure perturbation:

$$N = \frac{\int_{V,t} q'(V,t)p'(V,t)dt dV}{\int_{V,t} (p'(V,t))^2 dt dV}, \quad (19)$$

where the double integral is taken over the wave period of time  $t$  in the finite volume  $V$ . Considering now sinusoidal or harmonic oscillations that are uniform over a finite volume, the response factor  $N$  is reduced to  $N = (|\hat{q}'|/|\hat{p}'|)\cos\phi$ , where  $|\hat{q}'|$  and  $|\hat{p}'|$  stand for the modules of mass release  $q'$  and pressure  $p'$ , and  $\phi$  denotes the phase lag or i.e. the angle difference between  $q'$  and  $p'$ . Thus, in this case, a reduced mass response factor can be obtained as the real part of the mass transfer function  $Z = \hat{m}/(\alpha\hat{p}_C)$ . By using equations (15)-(18), the expression of the transfer function  $Z \equiv Z(u, \theta, h)$  is obtained as:

$$Z(u, \theta, h) = \frac{i u}{1 + i u} \frac{A + \theta E(u, \theta, h)}{B - \theta E(u, \theta, h)}, \quad (20)$$

where the involved thermodynamic coefficients  $A = 3(\bar{a}\bar{b} - \mu)/\lambda$  and  $B = 3\mu/\lambda$  depend on the fuel physical properties and are related to the ratio  $\lambda = (c_L \bar{T}_S)/\bar{\ell}$ . Then, the reduced mass response factor is the real part of the transfer function  $Z$  and will read:

$$\frac{N}{\alpha} = \Re(Z). \quad (21)$$

The reduced response  $N/\alpha$  will be briefly called “response factor” or “mass response factor” in the rest of the paper. It includes phase lag relations since it becomes positive when the vaporization rate and the chamber pressure are either above or below their mean values, and negative when the vaporization rate and the chamber pressure are on the opposite sides of their means [7]. Moreover, the phase lag or angle difference  $\phi$  between the vaporization rate and the chamber pressure, defined as the argument of the transfer function  $\phi = \arg(Z)$ , is proven to be insensitive to the chamber mean pressure magnitude [4]. Thus, the phase angle  $\phi$  appears to be one of the key parameters for analyzing the mass frequency response due to ambient pressure oscillations.

## 4. Results and discussion

### 4.1. General remarks

The values  $A = 10$  and  $B = 100$  will be used for the thermodynamic coefficients  $A$  and  $B$  in all calculations and curves, since they correspond respectively to orders of magnitude of values encountered in the classical fuels [15]. The effects of the heat transfer coefficient  $h$  on the mass response factor were pointed out in a recent publication by the same authors (see [26]). Those results will be briefly recalled and if necessary improved in the following subsection. Then, the response factor will be analyzed in relation to the process characteristic times as highlighted in Subsection 2.2, and to the phase angle  $\phi$  as defined in Subsection 3.3, and again to the influence of the value of the thermodynamic coefficient  $B$ .

In each diagram on Figures 2, 3, and 4, response factor curves are shown as function of the reduced frequency  $u = 3\omega\bar{\tau}_v$ , for a set of values of the exchange ratio  $\theta$ . For a given value of the heat

transfer coefficient  $h$ , a quite large number of values of the exchange ratio  $\theta$  are selected in order to illustrate a fairly wide range of curve profiles, among which the one related to a certain critical value of  $\theta$  to be later deduced in this analysis. The diagrams are ranged in columns corresponding respectively to six different values of the heat transfer coefficient:  $h = 0$  and  $h = 0.1$  for Figure 2;  $h = 1$  and  $h = 1.05$  for Figure 3;  $h = 10$  and  $h = +\infty$  for Figure 4. As already mentioned, the extreme values ( $h = 0$  and  $h = +\infty$ ) are connected to the adiabatic and isothermal feeding regimes and the related curves are here illustrated for comparison purposes with previous results obtained in [17]. Among the other selected values of the heat transfer coefficient ( $h = 0.1; 1; 1.05; 10$ ), the value  $h = 1$  is a critical value and can be roughly considered with the three other intermediate values as representative of the main types of curve profiles obtained for  $h$  varying from 0 to  $+\infty$ .

#### 4.2. Effects of the heat transfer coefficient

In [26], the evaporating mass response factor in a mixed injection regime has been analyzed in connection with the heat transfer coefficient  $h$  that controls this generalized feeding regime. The study has pointed out the following three main results.

First, it is noticeable that for  $h = 0$  (Figures 2(a1), 2(a2) and 2(a3)), and for  $h = +\infty$  (Figures 4(f1), 4(f2) and 4(f3)), the response factor curves seem very similar to those obtained respectively in the adiabatic and in the isothermal injection regimes, as discussed in [17]. In fact, calculations show that these curves are identical for a given value of the exchange ratio  $\theta$ , since, when  $h \rightarrow 0$ ,

$$E(u, \theta, h) \rightarrow \frac{\bar{s}_0 \bar{r}_S \theta \sin(\bar{s}_0 \bar{r}_S) + 2\theta \cos(\bar{s}_0 \bar{r}_S) - 3 \cos(\bar{s}_0 \bar{r}_S) - 2\theta + 3}{\theta (1 - \cos(\bar{s}_0 \bar{r}_S))} = E(u, \theta, 0). \quad (22)$$

While, as  $h \rightarrow +\infty$ ,

$$E(u, \theta, h) \rightarrow -\frac{1}{2} \frac{2\theta s_0 \bar{r}_S \sin(s_0 \bar{r}_S) + 5\theta \cos(s_0 \bar{r}_S) - 3 \cos(s_0 \bar{r}_S) - 5\theta + 3}{\theta (1 - \cos(s_0 \bar{r}_S))} = E(u, \theta, +\infty). \quad (23)$$

Thus, the expression of the function  $E(u, \theta, h)$  in equation (16), coincides with those obtained in [17], for the calculation of the complex transfer function  $Z(u, \theta, h)$  in the adiabatic and in the isothermal feeding regimes (respectively  $h = 0$  and  $h = +\infty$ ). Consequently, the results concerning the response factor curves in these two extreme regimes can be deduced as limiting cases from those of the present generalized injection regime. This kind of generalization has also been highlighted in a recent published paper (see [27]), where the mixed feeding regime was applied to a pastille-shaped droplet. Secondly, when the value of the heat transfer coefficient is fixed at one ( $h = 1$ ), the corresponding response factor curves show intriguing fluctuations in their profiles, as it can be observed on Figures 3(c1), 3(c2) and 3(c3). If in addition, the value of the exchange ratio is chosen less than one ( $\theta < 1$ ), that is for relatively small droplets, the fluctuations become straight chaotic as shown on Figure 3(c1). Nevertheless, these oscillations appear relatively reduced in amplitude compared to those obtained when the exchange ratio is much greater or equal to one ( $\theta \geq 1$ ). In the latter case, the response factor curves show hyperbolic patterns with more higher peak values along the frequency axis. But, once the heat transfer coefficient differs slightly from one, almost all the corresponding curves tend to show more lower fluctuations in their profiles, even if  $h$  remains very close to one as for example  $h = 1.05$  (see Figures 3(d1), 3(d2) and 3(d3)). The same behavior can be observed in the case where  $h = 0.95$ , case which is not illustrated with diagrams in the present paper. As comparison, a unity value of a heat transfer coefficient may characterize a heating from the flame towards the injection system through the chamber walls. According to [28], the radiative power is highly nonlinear and varies at the first order as the fourth power of the local instantaneous temperature. Likewise, in fuel injection processes, it may also be admitted that the evaporating mass frequency response

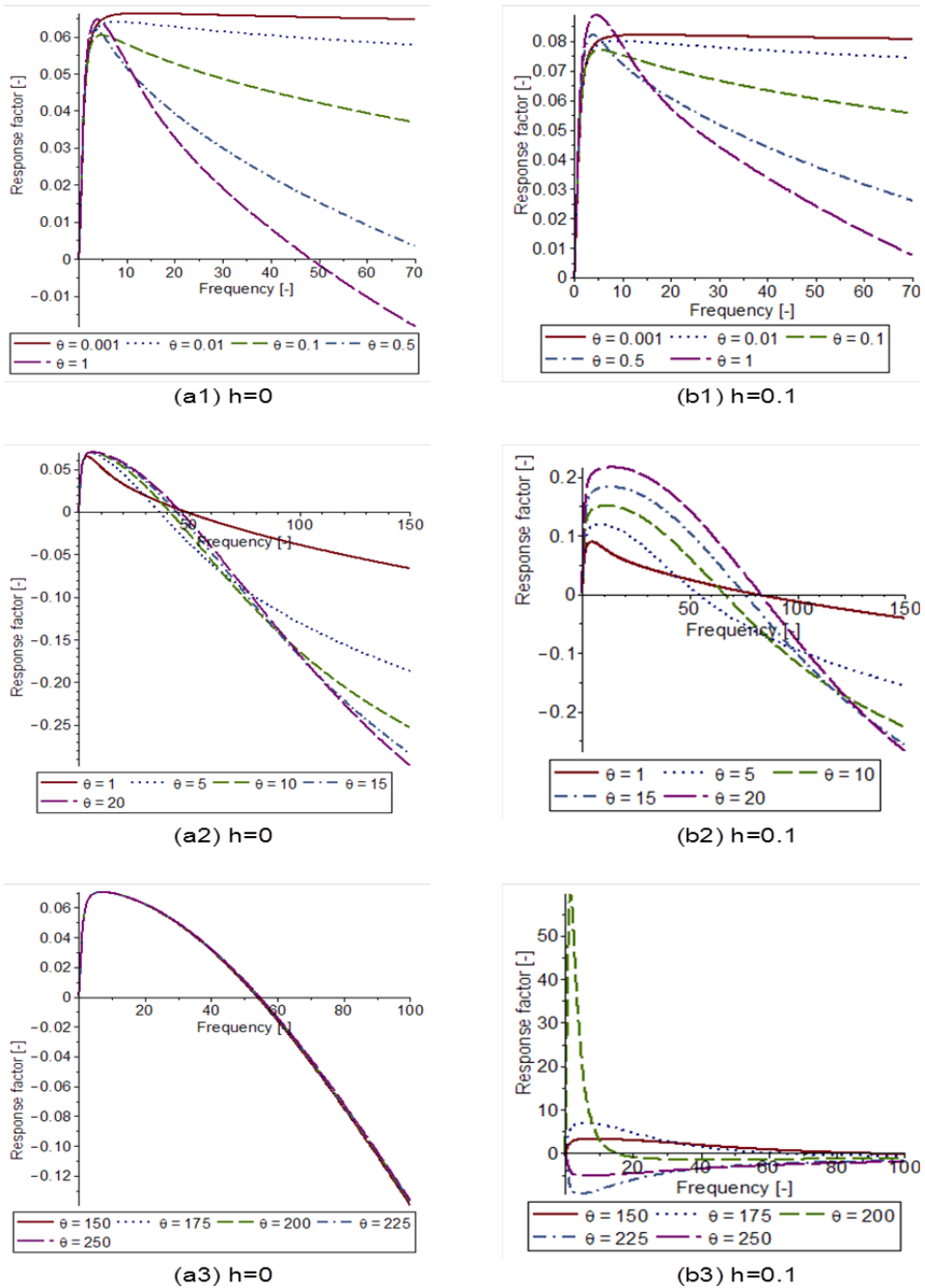


**Figure 2.** Mean droplet model with the thermodynamic coefficients  $A = 10$  and  $B = 100$ : Variation of the reduced response factor  $N/\alpha$  versus the dimensionless wave frequency  $u$  at various values of the non-dimensional exchange ratio  $\theta$  and for the heat transfer coefficients  $h = 0$  and  $h = 0.1$ .

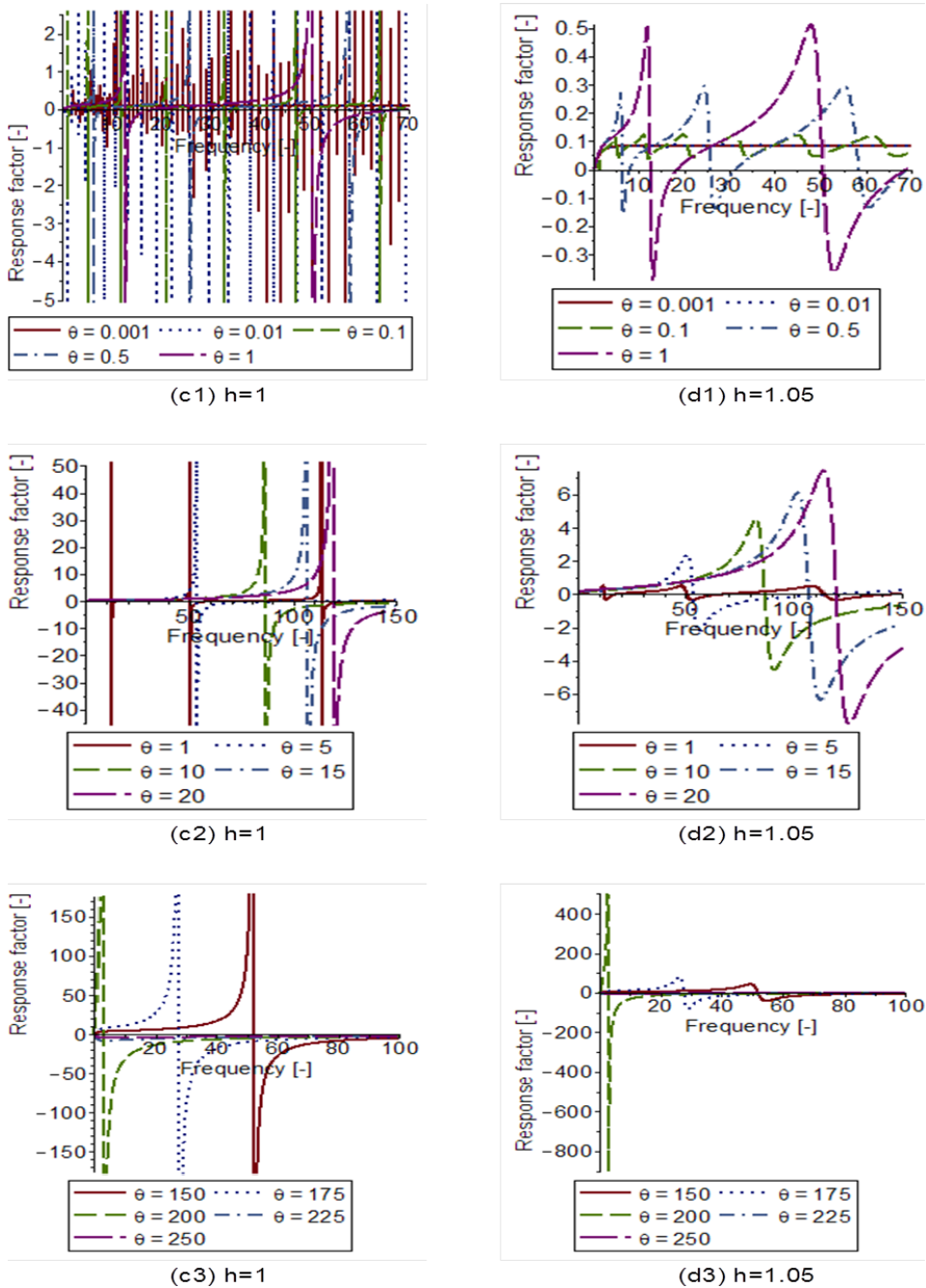


**Figure 3.** Mean droplet model with the thermodynamic coefficients  $A = 10$  and  $B = 100$ : Variation of the reduced response factor  $N/\alpha$  versus the dimensionless wave frequency  $u$  at various values of the non-dimensional exchange ratio  $\theta$  and for the heat transfer coefficients  $h = 1$  and  $h = 1.05$ .

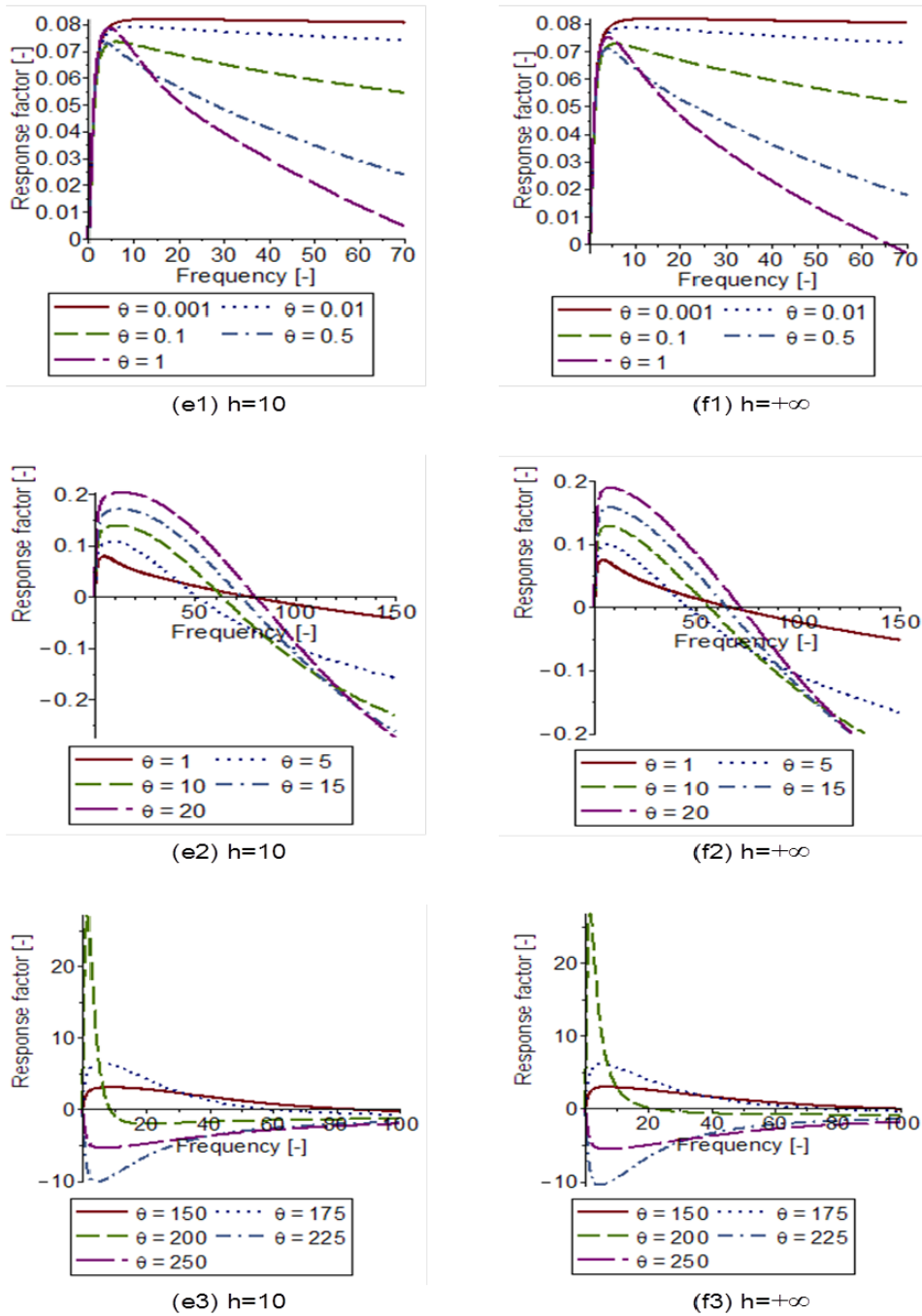


**Figure 4.** Mean droplet model with the thermodynamic coefficients  $A = 10$  and  $B = 100$ : Variation of the reduced response factor  $N/\alpha$  versus the dimensionless wave frequency  $u$  at various values of the non-dimensional exchange ratio  $\theta$  and for the heat transfer coefficients  $h = 10$  and  $h = +\infty$ .

of droplets and sprays can be strongly influenced near this specific value of the liquid-liquid heat transfer coefficient ( $h = 1$ ). Thirdly, the mass response factor curves for relatively large values of the heat transfer coefficient ( $h \geq 10$ ), seem to be very similar to those obtained in the isothermal injection regime ( $h = +\infty$ ). Indeed, the convergence of the function  $E(u, \theta, h)$  to  $E(u, \theta, +\infty)$  together with that of the corresponding response factor  $N/\alpha = \Re(Z)$  are proven to be asymptotic as  $h$  tends to  $+\infty$ . Thus, this convergence is approximately reached once the value of  $h$  is near 10, and the curves profiles on Figures 4(e1), 4(e2) and 4(e3) for  $h = 10$  seem to be identical to those on Figures 4(f1), 4(f2) and 4(f3) for  $h = +\infty$ .

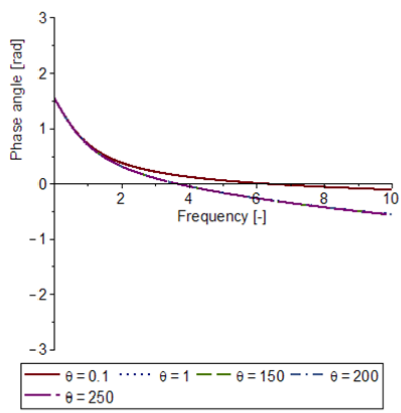
In brief, once the heat transfer coefficient becomes not null  $h > 0$  in the injection process, high and nonlinear instabilities may appear in the vaporization frequency response of droplets and sprays. As highlighted in [29, 30] among others, the process of continuous supply of fuel to the chamber has been theoretically and experimentally identified as an important factor for producing or driving combustion instabilities.

### 4.3. Effects of characteristic times and of the phase lag

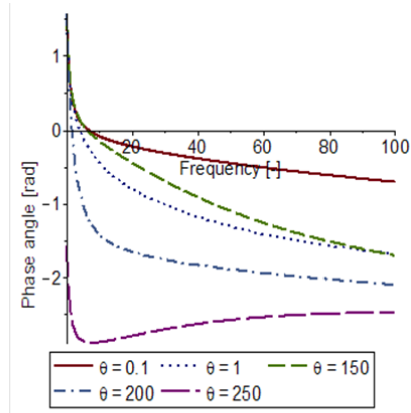
The vaporization response of a LOX droplet to oscillatory ambient conditions has been computed over a wide range of frequencies and the results were applied to prototypical cases pertinent to liquid rocket combustion instabilities [6]. It has been shown that the peak frequency for the computed response factor is correlated to the droplet lifetime. Indeed, as reported in [16, 17], the peak value of a response factor curve, whenever it exists, occurs at the same reduced frequency  $u_p$  that can be roughly evaluated about three. In mixed feeding regimes ( $h > 0$ ) as well as in both extreme cases of adiabatic and isothermal injection regimes, the peak frequency value can be estimated at  $u_p = 3\omega\bar{\tau}_v \approx 3$  (see among others, Figures 2(b1), 2(b2) for  $h = 0.1$  and Figures 4(e1), 4(e2) for  $h = 10$ ). This relation implies  $\bar{\tau}_v \approx 1/\omega$ , meaning that the injected liquid residence time  $\bar{\tau}_v$  is at the same order of magnitude as the pressure oscillation period  $1/\omega$ . Now, the mean residence time  $\bar{\tau}_v$  of a continuously fed droplet can be equated to the mean lifetime of free droplets in a spray. Therefore, whenever positive responses appear in the system, regardless of the value of the heat transfer coefficient  $h \geq 0$ , the vaporization rate can fully respond to the acoustic oscillations, only when the mean droplet lifetime is equal to the period of the ambient pressure oscillations.

It has also been anticipated that the well-known phase-lag model represents a key to a fundamental understanding of the evaporating mass frequency response to ambient pressure oscillations. Figure 5 shows phase angle curves ( $\phi = \arg(Z)$ ), as functions of the reduced frequency  $u = 3\omega\bar{\tau}_v$ , for selected values of the exchange ratio  $\theta$ . The curves are represented in a range of diagrams corresponding respectively to the same list of selected values of the heat transfer coefficient, namely  $h = 0; 0.1; 1; 1.05; 10$  and  $+\infty$ , as retained for the illustration of the response factor curves. For  $h = 0$ , that is in the adiabatic feeding regime (see Figure 5(a)), phase angle curves collapse in a single line once  $\theta \geq 1$ , in accordance with the response factor curve profiles obtained on Figures 2(a1), 2(a2) and 2(a3). It is also remarkable that the cut-off frequency of this single curve, at which the phase angle cancels, is approximately equal to the peak frequency  $u_p = 3\omega\bar{\tau}_v \approx 3$ , where the vaporization rate oscillates in phase with the acoustic pressure ( $\phi = 0$ ). In the adiabatic regime, a typical phase-angle curve starts from  $\pi/2$  at the frequency  $u = 0$ , where the mass response is null, decreases rapidly to zero at the cut-off frequency  $u_p$ , where the response is maximal, and then decreases asymptotically to a negative value about  $-\pi/3$ , expressing thus a progressive damp of instability in the system. Likewise, the phase-angle curves for  $h = 0.1; 1$  and  $1.05$  as shown on Figures 5(b), 5(c) and 5(d) are in agreement with the expectations. Indeed, when  $h = 0.1$  (see Figure 5(b)), each corresponding response factor curve on Figures 2(b1), 2(b2) and 2(b3) shows for the selected value of the exchange ratio  $\theta$ , a unique peak frequency  $u_p$  which

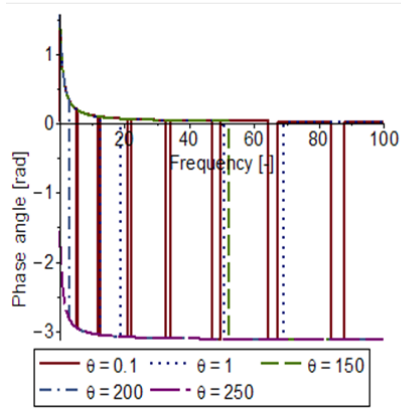




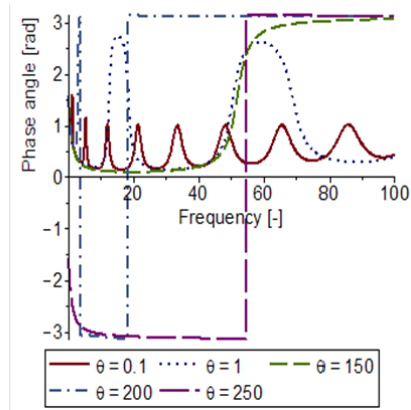
(a)  $h=0$



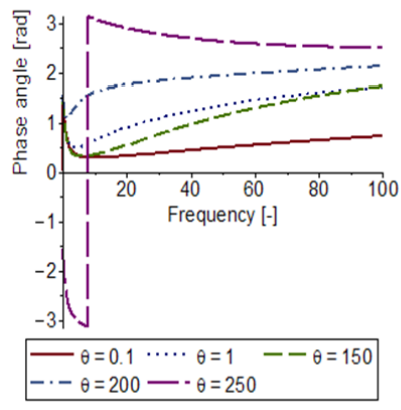
(b)  $h=0.1$



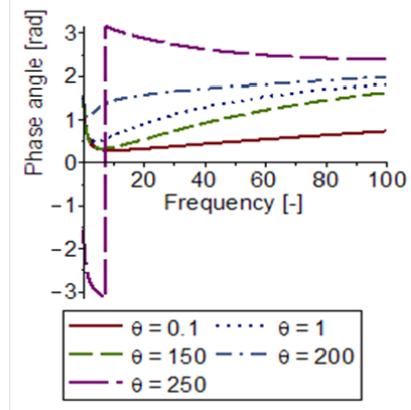
(c)  $h=1$



(d)  $h=1.05$



(e)  $h=10$



(f)  $h=+\infty$

**Figure 5.** Mean spherical droplet model with the thermodynamic coefficients  $A = 10$  and  $B = 100$ : variation of the phase lag  $\phi$  versus the dimensionless wave frequency  $u$  at various values of the non-dimensional exchange ratio  $\theta$  and for different value of the heat transfer coefficient  $h$ .

is relatively small. This leads to a reduced instability domain. A phase-angle curve on Figure 5(b) varies almost monotonously from the single peak frequency and remains inside a relatively limited range of values. On the contrary, except for  $\theta = 250$ , phase-angle curves for  $h = 1$  and  $1.05$  as represented on Figures 5(c) and 5(d), exhibit many fluctuations even from the lower bound  $-\pi$  to the upper bound  $\pi$  (see Figure 5(d) for  $\theta = 200$ ). Those profiles are in accordance with their respective response factor curves, as shown on Figure 3.

The phase-angle curve profiles obtained on Figure 5(e) for  $h = 10$  seem to be identical to those obtained in the isothermal feeding regime, i.e. on Figure 5(f) corresponding to  $h = +\infty$ . As mentioned in the subsection 4.2, this similitude is due to the asymptotic convergence of the response function, when  $h$  tends to  $+\infty$ . On the other hand, for  $\theta = 250$ , the phase-lag curve shows about the peak frequency  $u_p$ , an instantaneous change from the lower bound  $-\pi$  to the upper bound  $\pi$  as it can be observed on Figures 5(e) and 5(f).

#### 4.4. Influence of a thermodynamic coefficient

As they occur about a fixed value of the thermal exchange ratio ( $\theta \approx 200$ ), the sharp changes noted in the response factor curve profiles on Figures 2(b3), 4(e3) and 4(f3) are not related to some particular values of the heat transfer coefficient, but rather to these specific values of  $\theta$ . As in [17], those rapid changes in curve profiles around the reduced frequency  $u_p \approx 3$ , can be proven as depending on a specific value of  $\theta$ , which is connected to the value of the fuel thermodynamic coefficient  $B = 3\mu/\lambda$ . In order to determine the threshold value  $\theta_d$  of the thermal exchange ratio at which abrupt changes intervene in the curve profiles, the ratio  $x = u/\theta = \omega\bar{\tau}_T/3$ , may be particularly useful. Indeed, the thermal diffusion time  $\bar{\tau}_T$  and the frequency of the oscillating wave  $\omega$  do intervene in this ratio, but not the residence time  $\bar{\tau}_v$ . This ratio can then be assumed negligible at  $u_p = 3\omega_p\bar{\tau}_{vp} \approx 3$ , provided that the thermal transfer time by diffusion  $\bar{\tau}_T$  is negligible compared either to the oscillation period  $1/\omega_p$  or to the residence time  $\bar{\tau}_{vp}$ , since  $1/\omega_p \approx \bar{\tau}_{vp}$  at the peak frequency  $u_p$ . Therefore, taking  $h > 0$  and assuming  $u$  closer to  $u_p$ , the second-order truncated expansion of the transfer function  $Z(u, \theta, h)$  in the neighborhood of  $x = 0$  leads to the approximation:

$$Z(u, \theta, h) \approx \frac{i u \left( A + \frac{\theta}{2} - \frac{3}{2} \right)}{(1 + i u) \left( B - \frac{\theta}{2} + \frac{3}{2} \right)}. \quad (24)$$

This expression does not depend anymore on the heat transfer coefficient  $h$ . In consequence, when the feeding process is controlled by a not null heat transfer coefficient ( $h > 0$ ), the value of  $\theta$  around which response factor curves exhibit the sharp peak at the frequency  $u_p$ , can be deduced from the approximation (24) by equating the denominator of  $Z$  to zero. Thus,  $\theta_d = 2B + 3 = 203$  for  $B = 100$ . Moreover, once the value of  $\theta$  exceeds  $\theta_d$ , one has  $\Re(Z) \leq 0$  whenever  $h > 0$ , as it can be equally deduced from the same approximation (24). Therefore, the corresponding curves show only negative response for all frequencies as respectively shown on Figures 2(b3), 4(e3) and 4(f3) for  $h = 0.1; 10$  and  $+\infty$ . As in [4, 31], many publications have highlighted that the rapid variations of fluid thermophysical properties near critical and supercritical processes, are the major factor contributing to abrupt changes in the vaporization frequency response. Now, when  $h = 0$ , i.e. in the adiabatic regime, the computations lead to the following approximation:  $Z(u, \theta, 0) \approx iu(A - 3)/[(1 + iu)(B + 3)]$ . In this case, as  $B = 3\mu/\lambda > 0$ , the denominator of the transfer function and hence that of the response factor cannot be canceled, even when  $\theta \approx 200$ . This explains the absence of abrupt changes in the profiles of the response factor curves, regardless of the values of the thermal exchange ratio  $\theta$  and of the heat transfer coefficient  $h$  (see Figure 2(a3)).

## 5. Conclusions

By introducing a heat transfer coefficient in the liquid fuel injection process, this study has permitted to extend to a generalized feeding regime, the results of the pressure-coupled vaporization frequency response of spray droplets. The evaporating mass frequency response of a spray of repetitively injected droplets in the combustion chamber has been analyzed through the Heidmann analogy of a mean spherical droplet.

Using basic parameters in their dimensionless form, the effects of the liquid heat transfer coefficient and of the evaporation characteristic times, as well as those of the phase lag and of the thermal exchange ratio are found effective for driven or damped instabilities. It has been shown that, whenever positive responses appear in the system, the peak value is reached at a particular frequency, where the residence time of the mean droplet matches the period of the ambient pressure oscillations. Except for the cases where the heat transfer coefficient is closed to one, response factor curves exhibit a single maximal response at the peak frequency. This maximal response grows abruptly at the peak frequency if the thermal exchange ratio approaches a certain threshold value. The latter is shown to be equal to a simple affine function of a thermodynamic coefficient related to the injected fuel physical properties. Once this threshold value of the thermal exchange ratio is passed over, a factor curve shows only negative response for all frequencies, even in the case where the heat transfer coefficient is equal to one. The results are also found similar to those previously obtained in the adiabatic and isothermal feeding regimes. Indeed, mass response factors in such extreme cases of fuel injection are recovered as simple limit points.

On the theoretical level, the above-mentioned results may be beneficial for instability control in combustion processes and may also contribute to the modeling of liquid fuel propulsion systems as that of launcher engines for example. The dimensionless parameters provided by the linear analysis can be used to characterize the dynamic behavior of the vaporization process for a wide range of liquid fuels, especially when relatively large droplets are involved. Moreover, the present analytical approach may serve to improve the development of numerical codes, as for instance the Computational Fluid Dynamic (CFD) codes. However, this approximate analytical model based on the Heidmann analogy is still extendable to more complex configuration details.

## References

- [1] V. Nair, R. I. Sujith, "Multifractality in combustion noise: Predicting an impending instability", *J. Fluid Mech.* **747** (2014), p. 635-655.
- [2] T. Pant, C. Han, H. Wang, "Computational investigations of the coupling between transient flame dynamics and thermo-acoustic instability in a self-excited resonance combustor", *Combust. Theory Model.* **23** (2019), no. 5, p. 854-884.
- [3] S. Candel, D. Durox, T. Schuller, N. Darabiha, L. Hakim, T. Schmitt, "Advances in combustion and propulsion applications", *Eur. J. Mech. B Fluids* **40** (2013), p. 87-106.
- [4] G. C. Hsiao, H. Meng, V. Yang, "Pressure-coupled vaporization response of *n*-pentane fuel droplet at subcritical and supercritical conditions", *Proc. Combust. Inst.* **33** (2011), p. 1997-2003.
- [5] S. Lei, A. Turan, "Chaotic modeling and control of combustion instability due to vaporization", *Int. J. Heat Mass Transfer* **53** (2010), p. 4482-4494.
- [6] W. A. Sirignano, J.-P. Delplanque, C. H. Chiang, R. Bhatia, "Liquid-propellant droplet vaporization: A rate controlling process for combustion instability", in *Liquid Rocket Engine Combustion Instability* (V. Yang, W. E. Anderson, eds.), Progress in Astronautics and Aeronautics, vol. 169, AIAA Publishers, Reston, 1994, p. 307-343.
- [7] L. Magri, M. P. Juniper, J. P. Moeck, "Sensitivity of the Rayleigh criterion in thermoacoustics", *J. Fluid Mech.* **882** (2020), article no. R1.
- [8] A. Duvvur, C. H. Chiang, W. A. Sirignano, "Oscillatory fuel droplet vaporization: Driving mechanism for combustion instability", *J. Propul. Power* **12** (1996), p. 358-365.
- [9] L. Yuan, C. Shen, Z. Xinqiao, "Dynamic response of vaporizing droplet to pressure oscillation", *Heat Mass Transf.* **52** (2017), p. 711-723.

- [10] A. Y. Tong, W. A. Sirignano, "Oscillatory vaporization of fuel droplets in an unstable combustor", *J. Propul. Power* **5** (1989), p. 257-261.
- [11] M. d. I. C. García, E. Mastorakos, A. P. Dowling, "Investigations on the self-excited oscillations in a kerosene spray flame", *Combust. Flame* **156** (2009), p. 175-186.
- [12] C. T. Haddad, J. Majdalani, "Transverse waves in simulated liquid rocket engines", *AIAA J.* **51** (2012), p. 591-605.
- [13] J. B. Greenberg, D. Katoshevski, "Polydisperse spray diffusion flames in oscillating flow", *Combust. Theory Model.* **20** (2016), p. 349-372.
- [14] M. F. Heidmann, P. R. Wieber, "Analysis of frequency response characteristics of propellant vaporization", Nasa technical note, NASA, 1966, <https://ntrs.nasa.gov/api/citations/19670003840/downloads/19670003840.pdf>.
- [15] R. Prud'homme, M. Habiballah, L. Matuszewski, Y. Mauriot, A. Nicole, "Theoretical analysis of dynamic response of a vaporizing droplet to an acoustic oscillation", *J. Propul. Power* **26** (2010), p. 74-83.
- [16] K. Anani, R. Prud'homme, "Theoretical analysis of thermal conduction effect on frequency response of a perturbed vaporizing spherical droplet", *Flow Turbul. Combust.* **98** (2017), p. 503-522.
- [17] K. Anani, R. Prud'homme, M. N. Hounkonnou, "Dynamic response of a vaporizing spray to pressure oscillations: Approximate analytical solutions", *Combust. Flame* **193** (2018), p. 295-305.
- [18] S. Y. Slavyanov, W. Lay, "The Heun class of equations", in *Special Functions: A Unified Theory Based on Singularities*, Oxford Mathematical Monographs, Oxford University Press, New York, 2000, p. 97-160.
- [19] J. G. Lee, D. A. Santavica, "Experimental diagnostics of combustion instabilities", in *Combustion instabilities in gas turbine engines: Operational Experience, Fundamental Mechanisms, and Modeling* (T. C. Lieuwen, V. Yang, eds.), Progress in astronautics and aeronautics, vol. 481, AIAA Publishers, Reston, 2005, p. 481-529.
- [20] C. I. Sevilla-Esparza, J. L. Wegener, S. Teshome, J. I. Rodriguez, O. I. Smith, A. R. Karagozian, "Droplet combustion in the presence of acoustic excitation", *Combust. Flame* **161** (2014), p. 1604-1619.
- [21] F. Laurén, J. Nordström, "Practical inlet boundary conditions for internal flow calculations", *Comput. Fluids* **175** (2018), p. 159-166.
- [22] S. Bari, T. H. Lim, C. W. Yu, "Effects of preheating of crude palm oil (CPO) on injection system, performance and emission of a diesel engine", *Renewable Energy* **27** (2002), p. 339-351.
- [23] S. Mondal, A. Mukhopadhyay, S. Sen, "Effects of inlet conditions on dynamics of a thermal pulse combustor", *Combust. Theory Model.* **16** (2012), p. 59-74.
- [24] R. S. Miller, K. Harstad, J. Bellan, "Evaluation of equilibrium and non-equilibrium evaporation models for many droplet gas-liquid flow simulations", *Int. J. Multiphase Flow* **24** (1998), p. 1025-1055.
- [25] B. Abramzon, W. A. Sirignano, "Droplet vaporization model for spray combustion calculations", *Int. J. Heat Mass Transfer* **32** (1989), no. 9, p. 1605-1618.
- [26] K. Anani, R. Prud'homme, M. N. Hounkonnou, "Drop vaporization frequency response: an approximate analytical solution for mixed injection regimes", *Thermodynamics of Interfaces and Fluid Mechanics (TIFM)* **5** (2021), p. 1-11.
- [27] R. Prud'homme, K. Anani, "Vaporization of an equivalent pastille", in *Fluid Mechanics at Interfaces 2: Case Studies and Instabilities* (R. Prud'homme, S. Vincent, eds.), ISTE/Wiley Publishers, London, 2022, p. 77-93.
- [28] R. Gonçalves Dos Santos, M. Lecanu, S. Ducruix, O. Gicquel, E. Iacona, D. Veynante, "Coupled large eddy simulations of turbulent combustion and radiative heat transfer", *Combust. Flame* **152** (2008), p. 387-400.
- [29] Y. Xu, M. Zhai, P. Dong, F. Wang, Q. Zhu, "Modeling of a self-excited pulse combustor and stability analysis", *Combust. Theory Model.* **15** (2011), p. 623-643.
- [30] A. Kannan, B. Chellappan, S. Chakravarthy, "Flame-acoustic coupling of combustion instability in a non-premixed backward-facing step combustor: The role of acoustic-Reynolds stress", *Combust. Theory Model.* **20** (2016), p. 658-682.
- [31] J. Ren, O. Marxen, R. Pecnik, "Boundary-layer stability of supercritical fluids in the vicinity of the Widom line", *J. Fluid Mech.* **871** (2019), p. 831-864.